COUPLED CFD-GREEN'S FUNCTION APPROACH FOR PREDICTION OF COMBUSTION INSTABILITIES IN GAS TURBINES

Alessandra Bigongiari

School of Chemical and Physical Sciences, Keele University, Staffordshire ST55BG, UK
Dipartimento di Fisica, Università di Pisa, Largo Bruno Pontecorvo 3,56127, Pisa, Italy
email: a.bigongiari@keele.ac.uk

Maria Heckl

School of Chemical and Physical Sciences, Keele University, Staffordshire ST55BG, UK

Dmytro Iurashev

Università degli Studi di Genova, DICCA, via Montallegro 1, 16145

Many combustion systems, such as industrial gas turbine engines, are prone to suffering thermo-acoustic instabilities. This is a phenomenon where a feedback occurs between the acoustic waves and the heat release rate from the flame in a combustion chamber, generating pressure oscillations of high amplitudes, which in turn can cause serious damage to the combustor hardware. It is very important to predict under what conditions such instabilities occur and what oscillation amplitudes are reached. The aim of this paper is to present a fast prediction tool based on a one-dimensional Green's function approach that can be used to bypass numerically expensive computational fluid dynamics (CFD) simulations. We will demonstrate this tool by applying it to the case of a laboratory swirl burner. The flame will be modelled using a Flame Describing Function derived from full three-dimensional CFD simulations. Stability predictions will be compared with results obtained from three-dimensional simulations for selected operating conditions (limited by the high computational cost).

1. Introduction

The approaches to model thermoacoustic instabilities can be divided roughly into two groups:

(1) Low-order models describe a combustion system as a network of elements, connected by transfer functions or transfer matrices. Such models are largely analytical, they provide predictions with little numerical effort.

(2) Numerical simulations with CFD codes (URANS, LES) mimic the geometrical details of the combustion system, and capture the physical and chemical processes that occur in it, and hence they provide accurate quantitative predictions. However, they tend to be computationally expensive. In fact combustion modelling is a multiscale problem, with length scales ranging from less than 1 mm (flame front thickness) to more than 1 m (acoustic wavelength). In addition, the frequency to growth-rate ratio can be very large for an acoustic disturbance; this means that an unsteady CFD simulation of a slowly growing instability would necessitate the simulation of a large number of cycles, with high temporal accuracy.

In this paper we present a hybrid approach, which combines the advantages of both approaches: accurate predictions and low numerical cost. In order to illustrate our method, we consider the "BRS (Beschaufelter Ring-Spalt) burner" where methane is burnt in the lean combustion regime. The BRS test rig was initially developed by [1] at the Technische Universität München, and has been studied by different authors both experimentally [1] and numerically [2]. This is an atmos-

pheric test rig with a maximum power of 70 kW and a premixed methane/air swirl flame. The axial swirl generator is mounted on a central bluff body, and both serve to stabilise the flame. We will reconstruct the Flame Describing Function (FDF) from full three-dimensional CFD simulations of the BRS geometry, where the flame is excited acoustically. The results will then be used to perform a stability analysis based on a Green's function approach.

The Green's function approach is an analytical method which describes the combustion system in terms of a few parameters and captures the key physical aspects, giving stability predictions quickly and without much numerical effort.

2.   3-D simulations with CFD

The BRS set-up has a cylindrical burner tube (diameter 40 mm, length 16 cm), which is connected to a square combustion chamber (cross-section 90×90 mm^2, length 30 cm). A central rod (diameter 16 mm, length 16 cm), which spans the length of the burner tube, acts as a bluff body and makes the burner tube effectively annular. A swirler with 8 blades is mounted on the central rod.

This set-up is simulated numerically with URANS in an OpenFOAM environment. The flame is described by a flame speed closure model; this assumes a single-step chemical reaction, which is governed by the transport equation for the progress variable. Further details can be found in [6].

2.1   The Flame Describing Function

The FDF is an amplitude-dependent Flame Transfer Function (FTF), i.e. the response of the flame to a perturbation having a given frequency and amplitude. It relates the normalized fluctuations of the heat release rate to the normalized fluctuations of the acoustic velocity at a reference position upstream of the flame,

$$\text{FDF}(A,\omega) = \frac{\hat{Q}(A,\omega)/\bar{Q}}{\hat{u}_q(A,\omega)/\bar{U}} \ , \tag{1}$$

where $\hat{Q}$ and $\hat{u}_q$ are the fluctuations in the frequency domain of the heat release rate and velocity, respectively, and $\bar{Q}$ and $\bar{U}$ are the corresponding mean quantities.

The FDF is obtained experimentally by applying a harmonic perturbation at the inlet (usually through a loudspeaker or a siren) and recording the time histories of the acoustic velocity and heat release rate fluctuations. Spectral analysis then allows the calculation of the gain and phase of the FTF as a function of frequency and perturbation amplitude (see [5]).

We mimicked this experimental procedure by full CFD simulations. Velocity perturbations of different frequencies and amplitudes were imposed separately at the inlet. Time histories were obtained for the axial velocity $u_q(t)$ (area-averaged at the reference position, 2 cm upstream of the combustion chamber), and for the global heat release rate $Q(t)$ (volume integrated over the computational domain). The following 4 frequency values were tested: 100 Hz, 240 Hz, 160 Hz, 320 Hz. For the perturbation amplitude we took 3 values, expressed in terms of percentage of the mean velocity: 10%, 30%, 50% and 70%. Phase and gain of the FDF were obtained from the Fourier transform of the time histories $u'_q(t) = u_q(t) - \bar{U}$ and $Q'(t) = Q(t) - \bar{Q}$. The results are shown in Figure 1.

2.2   Analytical representation of the FDF

The FTF resulting from the numerical simulations has a gain which shows low-pass filter behaviour, and the phase is a nearly-linear function of frequency. In order to incorporate these FTF results into our Green's function approach, they need to be represented in analytical form.

2.2.1   Heat release law with time-lag distribution

We construct a heat release law, which is an extension of the well-known $n\tau$–law. It features distributions around two central time-lag values τ_1 and τ_2, two coupling coefficients n_1 and n_2, as well as the parameters σ_1 and σ_2, which specify the width of the distributions:

$$\frac{Q(t)}{\overline{Q}} = n_1 \int\limits_{\tau=0}^{\infty} \frac{u_q(t-\tau)}{\overline{U}} D_1(\tau-\tau_1)d\tau - n_2 \int\limits_{\tau=0}^{\infty} \frac{u_q(t-\tau)}{\overline{U}} D_2(\tau-\tau_2)d\tau . \tag{2}$$

The distributions are assumed to be Gaussian with standard deviations σ_1 and σ_2,

$$D_i(\tau) = \frac{2}{\sigma_i \sqrt{2\pi}} e^{-\frac{(\tau-\tau_i)^2}{2\sigma_i^2}} , \qquad i = 1,2 . \tag{3}$$
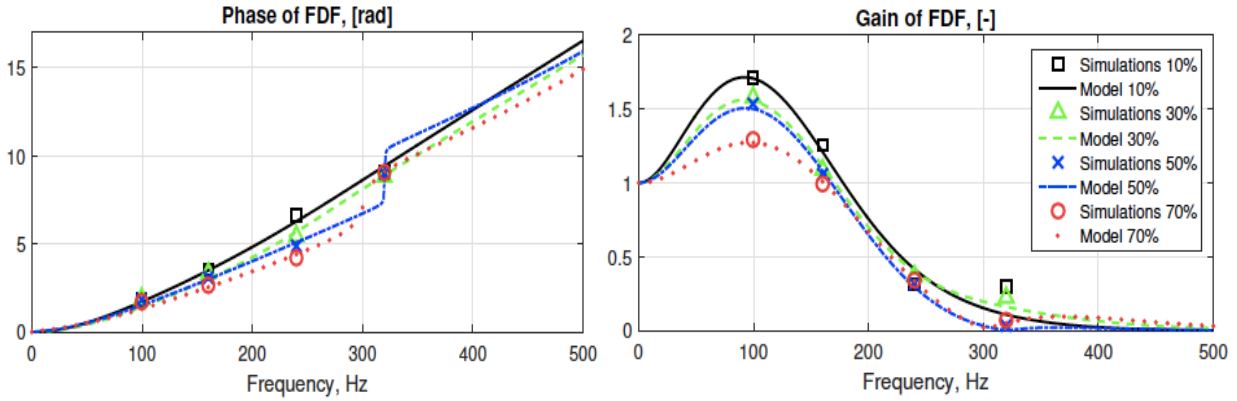
Figure 1: Phase (left) and Gain (right) of the FDF for different perturbation amplitudes. Symbols show the results obtained with CFD simulations. Smooth curves show the fitted results using the model equation (6) with fitting parameters from Table 1.

The heat release law described by Eq. (2) includes the $n\tau$ -law as special case, but it is much more versatile and able to capture a variety of physical effects:

(1) Heat release fluctuations may be induced by different physical effects, such as fluctuations in equivalence ratio, or vortex shedding at the flame holder. Such perturbations may travel with different speeds or over different distances, giving rise to two distinct time-lags in the flame response.

(2) Neighboring fluid particles may travel over slightly different distances and reach the flame front with slightly different delay times. This is included in our model by incorporating the distributions D_1 and D_2 .

2.2.2 Heat release law in the frequency domain

We denote the Fourier transform by $\mathcal{F}[\ ]$ and Fourier-transformed quantities by $\wedge$, e.g.

$$\mathcal{F}[Q(t)] = \frac{1}{2\pi} \int\limits_{t=-\infty}^{\infty} Q(t)e^{i\omega t}dt = \hat{Q}(\omega) . \tag{4}$$

For convenience, we assume that the distribution is such that $D_i(\tau-\tau_i) = 0$ for $\tau \leq 0$. This will then allow us to extend the range of integration in Eq. (4) from $[0, \infty]$ to $[-\infty, \infty]$ and calculate the Fourier transform of Eq. (2)

$$\frac{\hat{Q}(\omega)}{\overline{Q}} = n_1 \frac{\hat{u}_q}{\overline{U}} e^{i\omega\tau_1} e^{-\sigma_1^2 \omega^2/2} - n_2 \frac{\hat{u}_q}{\overline{U}} e^{i\omega\tau_2} e^{-\sigma_2^2 \omega^2/2} , \tag{5}$$

which gives the flame transfer function

$$FTF(\omega) = n_1 e^{i\omega\tau_1} e^{-\sigma_1^2 \omega^2/2} - n_2 e^{i\omega\tau_2} e^{-\sigma_2^2 \omega^2/2} . \tag{6}$$

2.2.3 Fitting function for the FDF results from our simulations

A comparison of the FTF in Eq. (6) with the data obtained from the CFD simulations (see Figure 1) shows that they have the same key features, in particular the excess gain and the low-pass behaviour. We can therefore take Eqn. (6) as a suitable analytical representation and fit it to the CFD results by careful choice of the six parameters $n_0, n_1, \tau_1, \tau_2, \sigma_1, \sigma_2$. In order to make sure that $|FTF|=1$ at $\omega = 0$, we choose $n_0 = n_1 - 1$. The remaining 5 parameters are chosen by minimising the mean square error, i.e. by minimising the expression

$$(\text{gain}_{CFD} - \text{gain}_{(6)})^2 + w \, (\text{phase}_{CFD} - \text{phase}_{(6)})^2 \qquad (7)$$

(w is a weighting factor to take into account that the phase has numerically higher values than the gain), averaged over the frequency interval $\omega = [0, \ldots 2\pi \times 500 \mathrm{s}^{-1}]$. The results are shown in Table 1.

Table 1: Fitting parameters

amplitude	n_1	n_2	$\tau_1[ms]$	$\tau_2[ms]$	$\sigma_1[ms]$	$\sigma_2[ms]$
10%	2.67	1.67	4.06	6.27	1.82	1.17
30%	1.94	0.94	3.10	6.00	1.63	0.92
50%	1.69	0.69	2.97	6.10	1.31	1.12
70%	1.38	0.38	2.48	5.76	1.14	0.72

We observe that the parameters $n_0, n_1, \tau_1, \tau_2, \sigma_1, \sigma_2$ are amplitude dependent. The data points for n_1 and n_2 are slightly scattered around a line with negative slope. We approximate them by a linear function of the perturbation amplitude:

$$n_1 = 2.74 - 2.05\frac{A}{U}, \quad , \quad n_2 = 1.74 - 2.05\frac{A}{U}. \qquad (8)$$

The data points for τ_1 and τ_2 also show a decreasing trend as the amplitude increases, and again we approximate this dependence by a linear function,

$$\tau_1 = 4.13 - 2.43\frac{A}{U}, [ms] \quad , \quad \tau_2 = 6.31 - 0.70\frac{A}{U}, [ms] \ . \qquad (9)$$

Similarly, the data points for σ_1 and σ_2 show a decreasing trend as the amplitude increases, and we approximate them by

$$\sigma_1 = 1.94 - 1.17\frac{A}{U}, [ms] \quad , \quad \sigma_2 = 1.21 - 0.57\frac{A}{U}, [ms]. \qquad (10)$$

3. Analytical model

3.1 The Green's function

The Green's function is the acoustic field generated in the tube at location x and time t by an impulsive point source located at x' and firing at t'. We denote it by $G(x, x', t, t')$ and describe it in terms of the velocity potential. Its governing equation is the non-homogeneous wave equation,

$$\frac{1}{c^2}\frac{\partial^2 G}{\partial t^2} - \frac{\partial^2 G}{\partial x^2} = \delta(x - x')\delta(t - t') \ , \qquad (11)$$

together with boundary conditions described by reflection coefficients R_0 at the inlet and R_L at the outlet. The Green's function is a superposition of modes, with modal amplitudes g_n and modal frequencies ω_n,

$$G(x, x', t, t') = H(t - t')\Re\sum_{n=1}^{\infty} g_n(x, x')e^{-i\omega_n(t-t')} \ . \qquad (12)$$

$H(t - t')$ denotes the Heaviside function. The quantities g_n and ω_n are calculated analytically for the specific set-up of the BRS burner.

3.2 Modelled configuration

In order to apply the Green's function approach to the BRS burner, we idealize the burner as shown in Figure 2. The burner tube is described as tube of constant cross-section S_1, with constant temperature $\overline{T}_1$; the combustion chamber has a larger cross-section S_2, and a constant temperature $\overline{T}_2 > \overline{T}_1$. The swirler is ignored; this is justified by the 3-D numerical simulations in [3] which show that the swirler does not influence the acoustic field significantly. We assume that the flame is compact and located at position x_q; this is downstream of the burner exit plane, which is located at x_j. In the burner tube, the speed of sound is c_1, and the mean density is $\overline{\rho}_1$. In the hotter combustion chamber, they are c_2 and $\overline{\rho}_2$. The choice of this temperature distribution was based on [4], where it is shown that modelling the temperature gradient of the compact flame does not produce significant changes in the results compared with a temperature jump. The boundary conditions at the tube ends are described by the reflection coefficients R_0 at the inlet and R_L at the outlet, which account for losses.
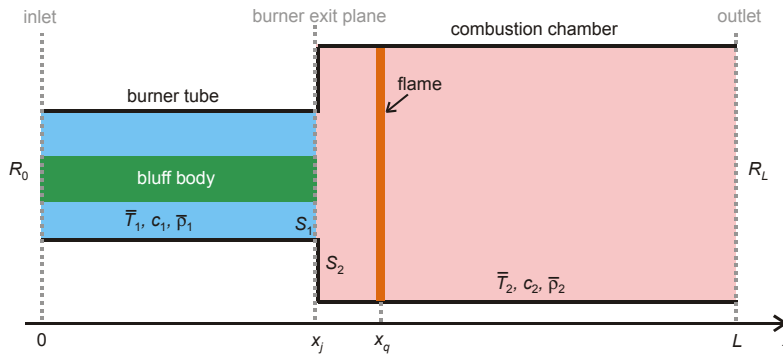
Figure 2: Schematic of the one-dimensional combustor under consideration.

3.3 Analytical form of the Green's function

Expressions for the modal amplitudes g_n of the Green's function in Eq. (2) have been calculated for the configuration described in section 3.2 (see [4, 10] for details on the derivation); the results are

$$g_n(x,x') = i \left. \frac{\hat{g}(x,x',\omega_n)}{\omega_n F(\omega_n)} \right|_{\substack{x=x_q \\ x'=x_q}} , \tag{13}$$

with

$$\hat{g}(x,x',\omega) = \begin{cases} D(x,\omega)C(x',\omega) & \text{for } x_j < x < x_q \\ C(x,\omega)D(x',\omega) & \text{for } x' < x < L \end{cases} \tag{14}$$

and

$$C(x,\omega) = e^{i\frac{\omega}{c_2}(x-L)} + R_L e^{-i\frac{\omega}{c_2}(x-L)}, \tag{15a}$$

$$D(x,\omega) = \frac{S_{ratio}}{2}\frac{c_2}{c_1}(R_0\, e^{i\omega\frac{x_q}{c_1}} - e^{-i\omega\frac{x_j}{c_1}})(e^{i\frac{\omega}{c_2}(x-x_j)} - e^{-i\frac{\omega}{c_2}(x-x_j)})$$

$$+ \frac{1}{2}\frac{\overline{\rho}_1}{\overline{\rho}_2}(R_0\, e^{i\omega\frac{x_q}{c_1}} + e^{-i\omega\frac{x_j}{c_1}})(e^{i\frac{\omega}{c_2}(x-x_j)} + e^{-i\frac{\omega}{c_2}(x-x_j)}). \tag{15b}$$

$$F(\omega) = \frac{S_{ratio}}{2}\frac{1}{c_1}[i(R_0\, e^{i\omega\frac{x_j}{c_1}} - e^{-i\omega\frac{x_j}{c_1}})(e^{i\omega\frac{x_j-L}{c_2}} + R_L e^{-i\omega\frac{x_j-L}{c_2}})$$

$$- i\frac{c_1}{c_2}\frac{\overline{\rho}_1}{\overline{\rho}_2}(e^{i\omega\frac{x_j-L}{c_2}} - R_L e^{-i\omega\frac{x_j-L}{c_2}})(R_0 e^{i\omega\frac{x_j}{c_1}} + e^{-i\omega\frac{x_j}{c_1}})]. \tag{16}$$

$F(\omega)$ is the function appearing in the characteristic equation, $F(\omega)=0$, which determines the modal frequencies ω_n in the Green's function. $S_{ratio} = S_1/S_2$ is the ratio of cross-sectional areas.

3.4 The integral equation

The velocity potential $\phi(x,t)$ of a sound field generated by a heat source with heat release rate $q(x,t)$ (per unit mass), can be described by the acoustic analogy equation

$$\frac{1}{c^2}\frac{\partial^2\phi}{\partial t^2}-\frac{\partial^2\phi}{\partial x^2}=-\frac{\gamma-1}{c^2}q(x,t) , \tag{17}$$

together with the initial conditions

$$\phi(x,t)\big|_{t=0}=\varphi_0\delta(x-x_q) \quad\text{and}\quad \frac{\partial\phi(x,t)}{\partial t}\bigg|_{t=0}=\varphi'_0\delta(x-x_q). \tag{18}$$

This set of equations can be converted into an integral equation for the acoustic velocity u with the use of the Green's function. For a compact heat source at $x=x_q$, described by

$$q(x,t)=q(t)\delta(x-x_q), \tag{19}$$

the integral equation is (see [9])

$$u_q(t)=\frac{\partial\phi}{\partial x}\bigg|_{x=x_q}=-\frac{\gamma-1}{c^2}\int_{t'=0}^{t}\frac{\partial G(x,x',t,t')}{\partial x}\bigg|_{\substack{x=x_q\\x'=x_q}}q(t')dt'-\frac{\varphi_0}{c^2}\frac{\partial G}{\partial x\partial t'}\bigg|_{\substack{x=x_q\\x'=x_q\\t'=0}}+\frac{\varphi'_0}{c^2}\frac{\partial G}{\partial x}\bigg|_{\substack{x=x_q\\x'=x_q\\t'=0}}. \tag{20}$$

It is worth noting that (20) is equivalent to the set of governing equations comprising (17), (18), and the boundary conditions described by R_0 and R_L.

In order to calculate the acoustic velocity from (20), we need an expression for the rate of heat release in terms of the acoustic field, i.e. we need the relationship that describes the acoustic feedback. This relationship is provided by the local heat release rate (per unit mass) based on Eq. (2),

$$q(t)=K\left[n_1\int_{\tau=0}^{\infty}u_q(t-\tau)D_1(\tau-\tau_1)d\tau-n_2\int_{\tau=0}^{\infty}u_q(t-\tau)D_2(\tau-\tau_2)d\tau\right], \tag{21}$$

where

$$K=\frac{\overline{Q}}{\overline{U}_2 S_2\overline{\rho}_2} \tag{22}$$

is the heater power per mass flow, having units Wskg^{-1}. As we found in section 2.2.3, the values of the time-lags τ_1, τ_2 and of the coupling constants n_1, n_2 are amplitude dependent. The inclusion of the amplitude-dependence is fundamental to the modelling of nonlinear effects, such as the formation of limit cycles. Our approach represents an advance compared with early nonlinear models, where an artificial saturation amplitude was imposed in order to "predict" limit cycles [7].

4. Stability maps

The integral equation (20) governs the evolution of the acoustic field in the presence of thermoacoustic feedback. From this equation it is possible to perform a modal analysis resembling an eigenvalue calculation that gives the frequencies of the acoustic modes driven by thermoacoustic feedback. The eigenmodes are determined by using a modal expression of for the acoustic velocity with complex amplitudes u_m and complex frequencies Ω_m,

$$u_q(t)=\sum_{m=1}^{\infty}\left(u_m e^{-i\Omega_m t}+u_m^* e^{i\Omega_m^* t}\right). \tag{23}$$

Equations for u_m and Ω_m are derived by combining Eq. (23) with the integral equation (20), the local heat release rate $q(t)$ in Eq. (21), and the modal expression for the Green's function in Eq. (12). We report here the equations for Ω_m obtained in [8] and extended to include the time-lag distribution.

$$\int_{\tau=0}^{\infty} e^{i\Omega_m\tau}\left[n_1 D_1(\tau) - n_2 D_2(\tau)\right]d\tau \sum_{n=1}^{\infty}\left[\frac{G_n}{i(\omega_n - \Omega_m)} - \frac{G_n^*}{i(\omega_n^* + \Omega_m)}\right] = -\frac{2c^2}{K(\gamma-1)}, \qquad (24)$$

with G_n given by

$$G_n = \left.\frac{\partial g_n(x,x')}{\partial x}\right|_{\substack{x=x_q, \\ x'=x_q}} . \qquad (25)$$

By solving Eq. (24) for Ω_m and then determining the sign of $\Im(\Omega_m)$, the stability behaviour of the burner can be predicted. We show the behaviour of mode 1 in the form of a stability map (see Figure 3) in the $L - A/\bar{U}$ plane. L (the combustor length) has been treated as control parameter and ranges from 0.36m to 2.26m; the amplitude $A/\bar{U}$ ranges from 0 to 1. The calculations were performed for the following boundary conditions: $R_0 = 1$ (rigid end at x=0) and $R_L = -1$ (open end at x=L), i.e. for a quarter-wave resonator without acoustic losses.
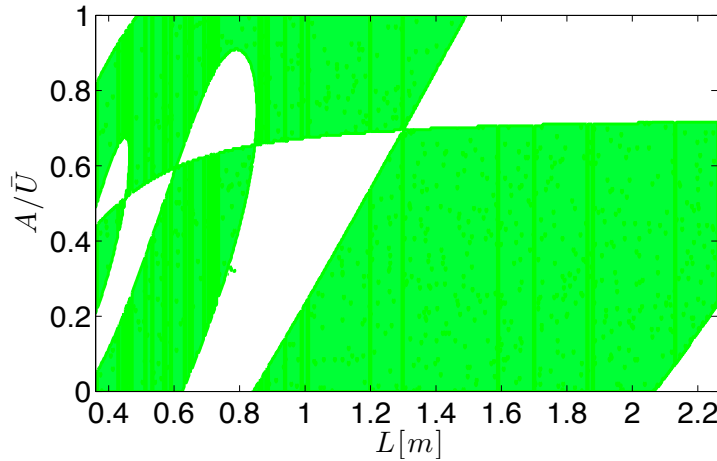
Figure 3: Stability map for the control parameter L.

Green areas indicate regions of instability: if the combustion system is such that the pair of values $(L, A/\bar{U})$ lies in an instability region, the perturbation will *grow* until $(L, A/\bar{U})$ reaches the border with the neighbouring stable region. White areas are regions of stability: if the point $(L, A/\bar{U})$ lies in such a region, the perturbation will *decay* in amplitude until the border with the next unstable region is reached. Interfaces between stable and unstable regions correspond to *limit cycles*: the growth rate of the perturbation is 0 for values of $(L, A/\bar{U})$ along the interfaces (see also [8]).

5. Validation

In order to validate our analytical results, we perform additional CDF simulations for the self-excited case. We choose the same boundary conditions as in the analytical model, and for the initial condition we take the profile of the 1st acoustic mode with several amplitudes. The calculated time histories for the velocity and pressure reveal the stability behaviour: if their amplitude increases, the burner is unstable, and otherwise it is stable. We performed the validation for the lengths L=0.84, 1.14 and 1.84m, and a perturbation amplitude $A/\bar{U}$ of 5%. Simulations for lengths L=0.84m and 1.84m show stable behaviour, whereas for L=1.14m the perturbation increases. This is shown in

figure 4. Therefore the simulations for L=0.84 and 1.14m agree with the predictions, while for L=1.84m we have a discrepancy. We suspect that the discrepancy is due to acoustic losses at the jump in cross-sectional area, which were included in the CFD simulations, but not in the analytical model; this point needs further investigation.

(a) (b) (c)
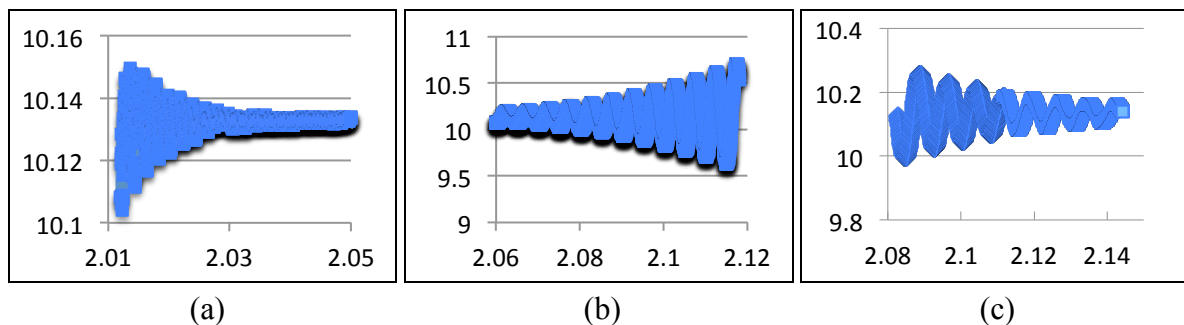
Figure 4: CFD results for the velocity time history for (a) L=0.84m, (b) L=1.14m and (c) L=1.84m.

6.   Conclusion

In this paper we have compared the predictions of the Green's function method with full three-dimensional CFD simulations. The Green's function method has the advantage of providing the stability boundaries fast and with a minimum of numerical effort. In addition it has a clear physical basis and describes the combustion system in terms of a few parameters and captures the key physical effects. The validation is currently work in progress, here we have presented the first results.

REFERENCES

1   Komarek, T., and Polifke, W. Impact of Swirl Fluctuations on the Flame Response of a Perfectly Premixed Swirl Burner, *J. Eng. Gas Turbines Power*, **132**, 061503-1,7, (2010).

2   Tay-Wo-Chong, L. and Polifke, W. LES-Based Study of the Infuence of Thermal Boundary Condition and Combustor Confinement on Premix Flame Transfer Functions, ASME paper GT2012-68796, (2012).

3   Iurashev, D. *PhD thesis*, Ansaldo Energia S.p.A., PDE/ISV/TMC/TFC, via N. Lorenzi 8, 16152 Genova, Italy, 30th March (2017).

4   Kosztin, B. *Linear and non-linear modelling of thermoacoustic instabilities in a laboratory burner*, PhD thesis, Keele University, (2013).

5   Noiray, N., Durox, D., Schuller, T. and Candel, S. A unified framework for nonlinear combustion instability analysis based on the flame describing function, *Journal of Fluid Mechanics* **615**, 139-167, (2008).

6   Iurashev, D., Campa, G. and Anisimov, V. Response of swirl stabilized perfectly premixed flame to high-amplitude velocity excitations, *23rd International Congress on Sound and Vibration*, Athens, Greece, 10-14 July, (2016).

7   Stow, S. R and Dowling, A. P., A time-domain network model for nonlinear thermoacoustic oscillations, *Journal of Engineering for Gas Turbines and Power* - Transactions of the ASME 131, article no 03150 (2009).

8   Bigongiari, A. and Heckl, M. 2015 A Green's function approach to the study of hysteresis in a Rijke tube. *Proceedings of the 22nd International Congress on Sound and Vibration*, Florence, Italy, 12-16 July, (2015) .

9   Heckl, M.A. and Howe, M.S. Stability analysis of the Rijke tube with a Green's function approach, *Journal of Sound and Vibration* **305**, 672-688, (2007).

10 Heckl, M.A. A new perspective on the flame describing function of a matrix flame, *International Journal of Spray and Combustion Dynamics* **7**, 91-112, (2015).